SOLAR WALLS FOR HIGH-PERFORMANCE BUILDINGS

BORISLAV N. STANKOV, NIKOLA G. KALOYANOV & GEORGI D. TOMOV
Technical University of Sofia, Bulgaria.

ABSTRACT

Passive solar design can reduce building energy demand for heating, cooling and ventilation, while also contributing to the comfort, well-being and productivity of the building's occupants. The successful application of passive solar features, such as solar walls, requires a good understanding of the factors influencing their energy performance and a correct assessment of this performance during the design process. This paper discusses some basic design strategies for successful application of solar walls and the factors with the most significant impact on their efficiency. It summarizes the principle results and findings of an experimental study, based on dynamic simulations and test site measurements. The energy performance of various configurations of unvented solar walls was investigated in different climatic conditions. The outcomes of the dynamic simulations were used to develop a simplified quasi-steady-state model, which can be used for approximate evaluation of the heat gains and heat losses through an unvented solar wall on a monthly basis. The model is compatible with the monthly method of EN ISO 13790.

Keywords: EN ISO 13790, energy performance, experimental, green buildings, heat transfer, modelling, passive solar, TRNSYS, Trombe wall.

1 INTRODUCTION

Passive solar design is a coalescence of design decisions concerning basic elements of building architecture, such as shape, orientation and spatial distribution, as well as individual passive systems or elements, which perform specific functions. The building envelope is a crucial element of passive solar design, as it determines the heat transfer processes occurring between the indoor and outdoor environments, including the ingress and distribution of solar radiation in the building. Solar walls can be employed as an element of passive solar design to enhance the capabilities of the building envelope to collect and store solar heat. The accumulated heat can be utilized to reduce the heating demand and/or provide means for natural ventilation.

Solar walls are also commonly referred to as 'Trombe walls' or 'Trombe–Michel walls', after the French engineer Felix Trombe and architect Jacques Michel, who developed a naturally ventilated type of solar wall [1]. A somewhat similar invention has been patented earlier by Morse [2]. Other sources use the terms 'collector-storage wall' or 'thermal storage wall' [3–5]. A solar wall consists of four basic elements: (1) thermal storage mass, i.e. wall; (2) absorber coating on the external surface of the wall; (3) glazing unit installed in front of the external surface of the wall; and (4) air gap between the wall and the glazing unit. The thermal storage mass is usually a solid masonry wall, built from a material which is relatively dense and has a high heat capacity. Examples include concrete, solid (non-porous) bricks, adobe and stone. Liquid-filled containers or encapsulated phase-change substances can be used to achieve greater thermal efficiencies [6, 7]. The absorber coating is a thin layer of material with very high solar absorptivity, e.g. black paint. A high-performance option is to use selective coating which has a very low infrared emissivity, e.g. black chrome [8–11]. Typically, the glazing unit would consist of one or two panes of clear glass, but other transparent materials are also possible. For example, Dowson *et al*. [12] investigate lightweight polycarbonate panels filled with nanoporous aerogel insulation as an alternative.

ISSN: 2056-3272 (paper format), ISSN: 2056-3280 (online), http://www.witpress.com/journals
DOI: 10.2495/EQ-V2-N4-339-351

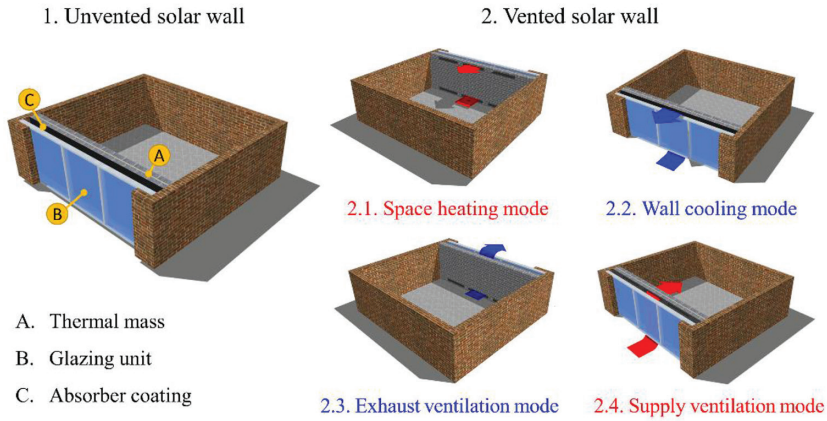

Figure 1: Basic configurations of solar walls.

A conceptual illustration of some basic solar wall configurations is shown in Fig. 1.

In an unvented solar wall heat absorbed at the external surface diffuses through the thermal storage mass and is transferred to the indoor environment with a time lag, which depends on the thermal diffusivity and thickness of the wall. When the solar wall is provided with vents, air can be allowed to flow through the space between the wall and the glazing. The absorption of thermal radiation produces a buoyancy-driven flow (solar chimney effect), whereby cold air entering through the bottom vents rises and gains heat from the absorber, and is subsequently discharged through the top vents. The air velocity and flow rate depend on the temperature differences and the pressure drops occurring through the vents and the air gap. Ventilation can be entirely natural or fan-assisted (if higher and/or constant flow rates are required). Saadatian *et al.* [6] gave a review of various traditional and innovative design concepts and applications of solar walls. Good examples of passive solar design incorporating solar walls can be found in the Zion National Park visitor centre and the NREL visitor centre in the United States [8, 9, 13].

This paper summarizes the principle results and findings of an experimental study on the energy performance of unvented solar walls of the classical type shown in Fig. 1. Therefore, further in this paper, the term 'solar wall' should understood in that context. The experimental study involves numerical analysis, based on dynamic simulations, and physical measurements obtained from a test site.

2 MATERIALS AND METHODS

2.1 Dynamic numerical model

The dynamic model was created in TRNSYS and consists of components from the TRNSYS standard library [14] and the TESS libraries [15], as well as an additional component, programmed for purposes of the experiment [16]. The basic component of the model is Type 36, which contains the method and algorithms for calculation of the heat flows and temperatures in the solar wall. The component is developed by the Solar Energy Laboratory of the University of Wisconsin-Madison [17].

2.1.1 Studied locations and solar wall configurations
Simulations were carried out for 11 340 configurations with variation of the following parameters:

- Thickness (10–50 cm) and material (Table 1) of the thermal storage mass;
- Type of absorber coating (Table 2);
- Type of glazing unit (one or two panes of clear glass);
- Distance between the wall and the glazing (in the range of 2.5–10 cm);
- Surface azimuth (-45°, 0° and +45°);
- Weather data (five locations in Bulgaria).

These simulations comprise the training set, which was used to develop the simplified model. A number of additional simulations were carried out with hourly weather data for 15 different locations in Europe and North America: Valencia, San Francisco, London, Rome, Istanbul, Richmond, New York, Munich, Strasbourg, Boulder, Chicago, Albuquerque, Stockholm and Helsinki. The selected locations are situated in diverse climate zones – ASHRAE climate zones 3 to 7 [18] and zones Csa, Csb, Cfa, Cfb, Dfa, Dfb and BSk, according to the Köppen–Geiger classification [19]. For comparison, four of the locations in Bulgaria (Pleven, Varna, Plovdiv and Sandanski) are situated in ASHRAE climate zone 4 and Köppen–Geiger zone Cfa, while the fifth (Sofia) is situated in ASHRAE zone 5 and Köppen–Geiger zone Cfb. The additional simulations (test set) were used to test and prove the robustness of the developed model and its validity for a wider range of climatic conditions. The test set consists of 4 320 data points.

2.1.2 Simulations and data processing
Each solar wall configuration was simulated twice. In the first instance, it was simulated with no incident solar radiation. In that case heat transfer through the solar wall is driven

Table 1: Properties of thermal storage materials.

Material	Thermal conductivity, [W/(mK)]	Density, [kg/m^3]	Specific heat capacity, [J/(kgK)]
Adobe	0.75	880	1730
Clinker brick	0.85	840	1500
Calcium-silicate brick	1.5	840	2000
Sandstone	1.3	712	2200
Limestone	1.5	720	2180
Concrete	1.7	840	2000

Table 2: Properties of absorber coatings. *(Source: Steven Winter Associates [11])*

Type of coating	Solar absorptivity	Infrared emissivity
Unfinished concrete	0.65	0.87
Flat black paint	0.96	0.87
Selective (black chrome)	0.95	0.11

only by the temperature difference between the indoor and outdoor environments, $Q_{ht,sw}$ (for simplicity, the term further used for $Q_{ht,sw}$ is 'heat losses', although heat flow driven by the indoor-outdoor temperature difference can occur in both directions). The second simulation was used to obtain the actual net heat transfer when solar radiation is taken into account. The solar heat gains through the wall, $Q_{gn,sw}$, were calculated as the difference between the net heat transfer obtained from the second simulation and the heat losses obtained from the first simulation. Equivalently, the net heat transfer between the solar wall and the indoor environment, Q_{sw}, [kWh], is equal to the difference between the heat gains and the heat losses:

$$Q_{sw} = Q_{gn,sw} - Q_{ht,sw}. \quad (1)$$

Both Q_{sw} and $Q_{ht,sw}$ can be positive or negative, while $Q_{gn,sw}$ can only be positive.

2.2 Test site configuration

The test site, shown in Fig. 2, comprises an unvented solar wall integrated in the south façade of a modular house, which is located at the Technical University of Sofia. The solar wall is built of a 12-cm-thick masonry wall with black paint as absorber coating and a clear double glazing, installed at 10 cm from the wall. The wall is divided in two parts – the lower half is made of concrete masonry, while the upper half is made of clay bricks. The test module is equipped with 28 type T thermocouples for measuring the temperature field in the wall and four sensors for measuring the temperatures and air velocities in the air space (Fig. 3). The nearby located weather station provided all necessary weather data, including measurements of total and diffuse solar radiation. Measurements were collected for the heating season of 2014/2015 (22 October–22 April).

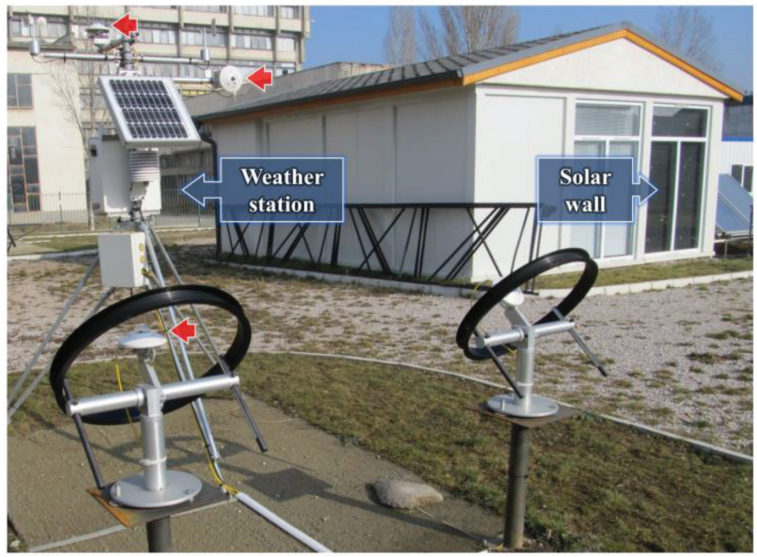

Figure 2: Test site at the Technical University of Sofia.

Figure 3: Configuration of the solar wall test module.

3 RESULTS AND DISCUSSION

The outcomes of the simulations were used to develop a simplified quasi-steady-state model, which can be used for approximate evaluation of the heat gains and heat losses through a classical unvented solar wall. The model is compatible with the monthly method of EN ISO 13790 [20]. It is presented here along with a discussion of the basic factors determining the energy performance of the solar wall and its sensitivity to their values.

Heat losses (as defined in section 2.1.2) can be calculated as:

$$Q_{ht,sw} = U_t A_{sw} \left(\theta_{int,set} - \theta_e\right) t \,/\, 1000. \tag{2}$$

where: $Q_{ht,sw}$ – heat losses, [kWh]; U_t – overall heat transfer coefficient of the solar wall, [W/(m^{2}K)]; A_{sw} – internal surface area of the wall, [m^2]; $\theta_{int,set}$ – internal set-point temperature, [°C]; θ_e – mean ambient temperature, [°C]; t – duration of the period, [h]. The overall heat transfer coefficient in eqn (2) is used to calculate the theoretical heat losses which will occur in the case of a complete lack of solar radiation (in order to separate the heat losses from the solar heat gains):

$$U_t = 1 / \left(R_{si} + L_p / k_p + 1 / U_e\right). \tag{3}$$

where: R_{si} – thermal resistance of the internal surface, [m^{2}K/W]; L_p – thickness of the wall, [m]; k_p – thermal conductivity of the wall, [W/(mK)]; U_e – external heat loss coefficient, [W/(m^{2}K)]. The thermal resistance of the internal surface accounts for the convective and radiative heat transfer between the surface and the indoor environment. Its value can be taken as 0.13 m^{2}K/W [21]. In the presence of additional material layers on the inside of the thermal storage mass, e.g. plastering, the thermal resistance of those layers should also be included.

The indirect solar heat gains through the solar wall can be calculated, in accordance with the common equation of EN ISO 13790 [20], as:

$$Q_{gn,sw} = F_{sh,ob} A_{sol,sw} I_{sol} t \,/ 1000. \tag{4}$$

where: $F_{sh,ob}$ – shading reduction factor for external obstacles (including terrain, nearby buildings, fixed external shading devices, etc.), [-]; I_{sol} – mean total solar irradiation on a surface with the corresponding slope and azimuth, [W/m^2]; $A_{sol,sw}$ – effective collecting area of the solar wall, [m^2].

The effective collecting area is expressed as a geometric factor, but its value depends on both geometric and non-geometric parameters. It represents the fraction of incident solar radiation that reaches the indoor environment as heat gains, after all reductions due to shading, reflection and heat losses to the outdoor environment:

$$A_{sol,sw} = F_{sh,gl} \left(1 - F_F\right) g_w \alpha_{ab} A_{sw} \eta_{sw}. \tag{5}$$

where: $F_{sh,gl}$ – shading reduction factor for movable shading provisions, [-]; F_F – frame area fraction (ratio of the projected frame area to the overall projected area of the glazing), [-]; g_w – total solar energy transmittance of the glazing unit, [-]; α_{ab} – solar absorptivity of the absorber coating, [-]; A_{sw} – internal surface area of the wall, [m^2]; η_{sw} – effective solar transmittance of the wall, [-].

The external heat loss coefficient accounts for all mechanisms of heat transfer occurring in the direction from the external surface of the wall, i.e. the absorber, to the outdoor environment. Appropriate values for the external heat loss coefficient have been extracted from the simulation outcomes using CART analysis. The most significant parameters, determining the value of this coefficient, are the infrared emissivity of the absorber coating and the type of glazing. The obtained values are given in Table 3.

The effective solar transmittance of the wall is a dimensionless factor, representing the fraction of absorbed solar radiation which reaches the indoor environment. It therefore accounts for the absorbed solar heat which is lost to the outdoor environment. Theoretically, this factor can vary between 0 and 1, while the values obtained from all simulations are in the range of 0.21 to 0.87 (with a median of 0.54). The following equation for calculation of η_{sw} was obtained through nonlinear regression analysis:

$$\eta_{sw} = \eta_{sw,0} - \left(0.105 - 0.026 k_p\right) ln\left(\tau_p\right). \tag{6}$$

$$\eta_{sw,0} = 0.915 - 0.227 ln\left(U_e\right). \tag{7}$$

Table 3: Values of the external heat loss coefficient – statistical summary.

		External heat loss coefficient, U_e, [W/(m^{2}K)]		
Absorber coating	Glazing	Average value	Median value	Median absolute deviation
Non-selective (ε_{ab} = 0.87)	Single clear	3.2	3.3	0.30
Non-selective (ε_{ab} = 0.87)	Double clear	2.1	2.1	0.16
Selective (ε_{ab} = 0.11)	Single clear	1.1	1.1	0.08
Selective (ε_{ab} = 0.11)	Double clear	0.9	0.9	0.06

where: k_p – thermal conductivity of the wall, [W/(mK)]; U_e – external heat loss coefficient, [W/(m^{2}K)]; τ_p – time-constant of the wall, which indicates its thermal inertia, [h]:

$$\tau_p = (\rho c)_p L_p^2 / (3600 k_p). \quad (8)$$

where: L_p – thickness of the wall, [m]; $(\rho c)_p$ – volumetric heat capacity of the thermal storage mass, [J/(m^{3}K)].

For consistency, eqn (7) was designed to use the same values for the external heat loss coefficent as eqn (3), i.e. the values given in Table 3. It should be noted, however, that the actual mean value of the external heat loss coefficient will be higher in the presence of solar irradiation, due to the increased temperature of the absorber. A statistical summary of the nonlinear regression model of eqn (6) is shown in Table 4. The functional relationships of eqns (6) and (7) are illustrated graphically in Figures 4 and 5.

During the heating season, some heat gains enter the building when no heating is needed. They may lead to an undesired increase of the internal temperature above the set-point, i.e.

Table 4: Statistical summary of the effective solar transmittance model.

Fitted equation: $\eta_{sw} = \zeta_1 - \zeta_2 ln(U_e) - (\zeta_3 - \zeta_4 k_p) ln(\tau_p)$.

		95% Confidence limits				
	Value	Lower	Upper	Standard error	t-value	Pr(>|t|)
ζ_1	0.9150	0.91472	0.91532	0.00015	5996	$< 2 \times 10^{-16}$
ζ_2	0.2274	0.22716	0.22758	0.00011	2127	$< 2 \times 10^{-16}$
ζ_3	0.1046	0.10442	0.10469	0.00007	1519	$< 2 \times 10^{-16}$
ζ_4	0.0265	0.02644	0.02663	0.00005	558.4	$< 2 \times 10^{-16}$

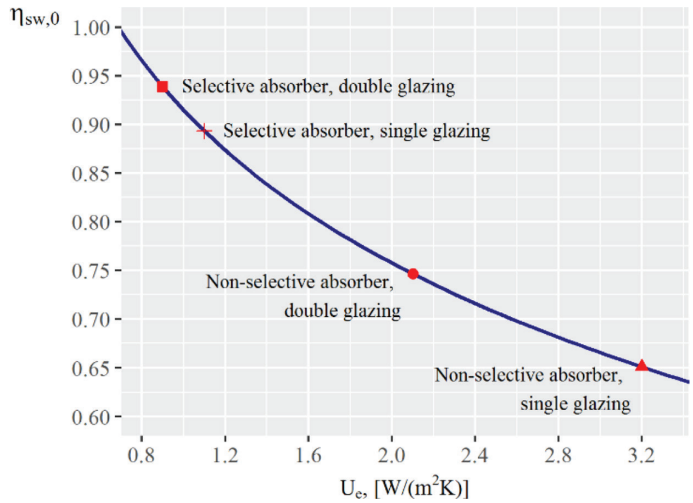

Figure 4: Variation of effective solar transmittance with external heat loss coefficient.

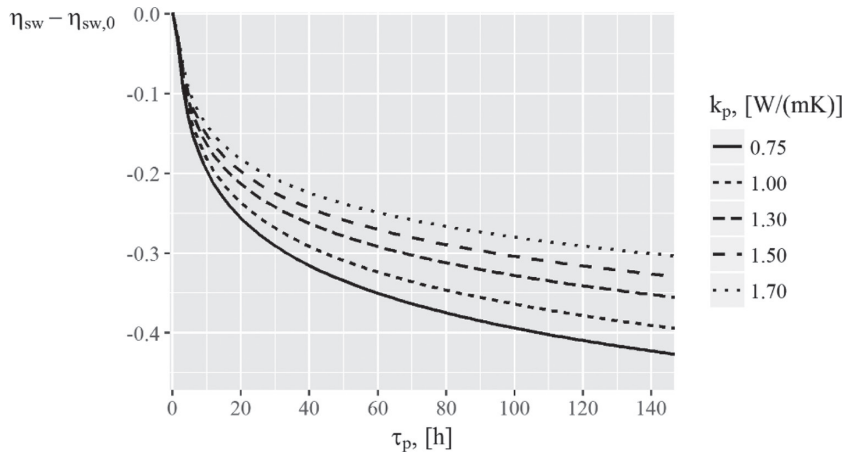

Figure 5: Variation of effective solar transmittance with thermal mass properties.

overheating. Such extra heat gains do not contribute to the reduction of building heating demand. The amount of heat gains, which are utilized for reducing the heating demand, depends on the total heat capacity of the respective thermal zone in the building. The higher the heat capacity – the greater the capability of the building to utilize the incoming heat gains (thermal storage enables a more even distribution of the heating loads in time). An analogous situation occurs in the summer when not all heat losses contribute to reduction of cooling demand. Therefore, according to the monthly method of EN ISO 13790 [20], for each building thermal zone and each calculation step (month), the energy demands for space heating, $Q_{H,nd}$, and cooling, $Q_{C,nd}$, are calculated as:

$$Q_{H,nd} = Q_{H,ht} - \eta_{H,gn} Q_{H,gn}. \tag{9}$$

$$Q_{C,nd} = Q_{C,gn} - \eta_{C,ls} Q_{C,ht}. \tag{10}$$

where: Q_{ht} – total heat transfer, [kWh]; Q_{gn} – total heat gains, [kWh]; $\eta_{H,gn}$ – dimensionless utilization factor for heat gains; $\eta_{C,ls}$ – dimensionless utilization factor for heat losses.

If the presented model is used in the context of whole-building energy analysis with the monthly method EN ISO 13790, heat losses and heat gains through the solar should be calculated separately and then each should be included in the building thermal zone's sum total of heat losses and heat gains. The heat capacity of the wall should be accounted for when calculating the internal heat capacity of the building thermal zone. The latter is used for computation of the dimensionless heat gains and heat losses utilization factors, as described in the standard [20].

Figure 6 shows comparison between the steady-state model and the test set. The plot on the left side shows the values obtained for the net heat transfer (eqn (1)) per unit area of the solar wall, with each data point representing one of all simulated solar wall configurations. In general, the observations are within an acceptable range from the diagonal line (which represents ideal coincidence). The histogram on the right side shows the distribution of the relative error. The histogram shows that for more than 90% of all data points the relative error is <15%. The median value of the relative error over the whole test set is 3.4%. However, this does not

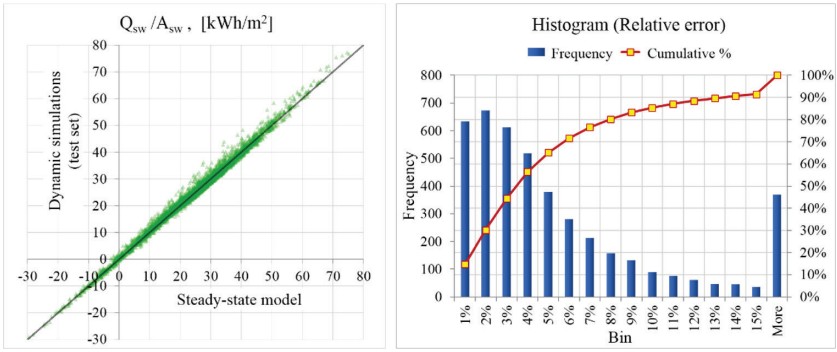

Figure 6: Accuracy of the steady-state model on the test set.

include errors which would arise when calculating the total solar energy transmittance of the glazing and the shading reduction factors of eqns (4) and (5).

The overall heat transfer coefficient and the effective solar transmittance are key factors for the energy performance of the solar wall. Both eqns (3) and (7) feature the external heat transfer coefficient, as well as the thermal conductivity, volumetric heat capacity and thickness of the thermal storage mass. The net heat transfer, as defined in eqn (1), is much more sensitive to the external heat loss coefficient than to the properties of the thermal storage material. A 10% change in the value of the thermal conductivity or the volumetric heat capacity of the wall results in only about 3% change in the output value, while a 10% change in the external heat loss coefficient results in more than 15% change in the output. The type of absorber coating and the type of glazing greatly influence the external heat loss coefficient and thereby the energy performance of the solar wall. It can be substantially improved if a selective absorber coating is used. Analysis of the experimental outcomes shows that, in such a case, the solar wall can significantly outperform a well-insulated external wall [16]. If the coating is not selective, it should be combined with double glazing. Configurations with no absorber coating and single glazing have very low efficiencies in moderate and cold climates.

On the other hand, the distance between the wall and the glazing unit exhibits little influence on the external heat loss coefficient in the range of investigated values. However, this distance should preferably be limited to 2–5 cm, to minimize shading on the absorber (i.e. reduce the value of F_F in eqn (5)). While the properties of the thermal storage material do not have a significant influence on the net heat transfer (results become slightly better when increasing the thermal resistance), they have a significant influence on the utilization of heat gains. In general, but not always, better overall performance should be obtained when the time-constant and the heat capacity of the thermal storage mass are higher [16]. The optimal time-constant may be dependent on the desired distribution of heat gains in time (a higher time-constant results in slower response to temperature variations).

For optimal performance, the solar wall should be facing south (in the Northern hemisphere) and to the maximum extend remain unshaded during the winter. Deviation of the surface azimuth of ±45° from due south reduces the efficiency of the solar wall by about 20% [16]. During the summer, however, it is necessary to provide efficient shading of the unvented solar wall to prevent undesirable heat gains. Fixed (e.g. overhangs) or movable exterior shading devices can by applied for this purpose, as well as natural shading if possible. A movable

external shading device would be the most efficient option, as it is the most controllable, while an overhang would be a simpler and cheaper solution. If an overhang is used, the projection length and angle should be carefully selected, because there will be a trade-off between allowing more solar radiation to pass in the heating season and allowing less in the summer. The optimal geometry of an overhang depends on the geometry and orientation of the solar wall, as well as the geographic latitude of the site. With good shading provided, the heat capacity of the wall could (if possible) be used as a device for heat load levelling, thereby reducing the required cooling capacities.

Additional insights were obtained through the physical measurements from the test site. A season-average daily profile of the temperatures in the upper half of the test site wall is shown in Fig. 7 (θ_1 and θ_7 are the external and the internal surface temperatures accordingly; the other temperatures are measured at equal distances in between; $\theta_{1(sh)}$ is the average temperature of the shaded area of the external surface). The profile was created by calculating the average values of the measured temperatures for each hour of the day over the entire heating season (22 October 2014–22 April 2015). Analysis of the measurements indicates that, as a rough estimate, the peak temperature is shifted by 20 minutes for each centimetre of added thickness. Comparison of the temperatures in the upper and lower halves of the wall demonstrates the effect of increasing the time-constant (which is about two times higher for the upper half, primarily due to the lower thermal conductivity of the clay bricks).

As heat diffusion is faster in the lower half, the amplitudes of its internal temperature are higher, while the differences between the internal and external surface temperatures are lower. As previously mentioned, increasing the thermal inertia of the wall delays and decreases the extremums of the internal surface temperature. This reduces the risk of causing thermal discomfort to the occupants of the building, which may arise due to radiant temperature asymmetry. According to ASHRAE Standard 55, the radiant temperature asymmetry should not exceed 10 K, if it is caused by a cold wall, or 23 K, if it is caused by a warm wall [22]. A histogram of the internal temperatures of each half of the wall, showing the number of hours (frequency) during which the internal surface has experienced the given temperature (bin), is shown in Fig. 8. The histogram indicates that in moderate climatic conditions, such as those in Sofia, the solar wall should not be a cause of thermal discomfort, except in rare cases. The risk will be increased if the wall is very thin and has a low time constant.

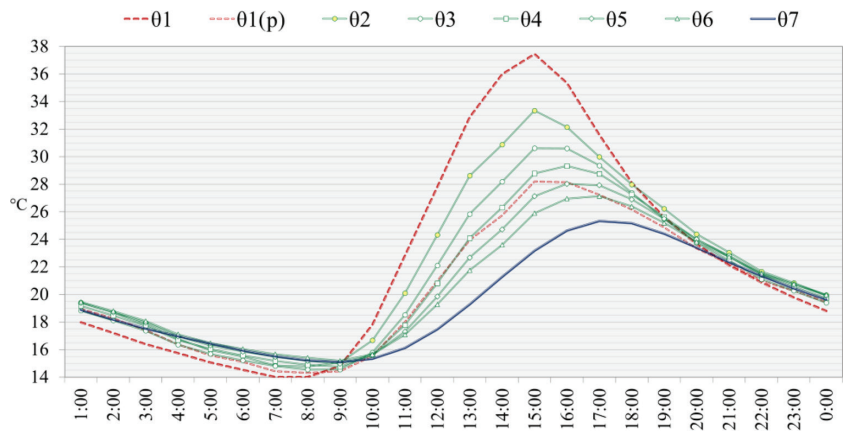

Figure 7: Season-average daily profile of the temperatures in the upper half of the wall.

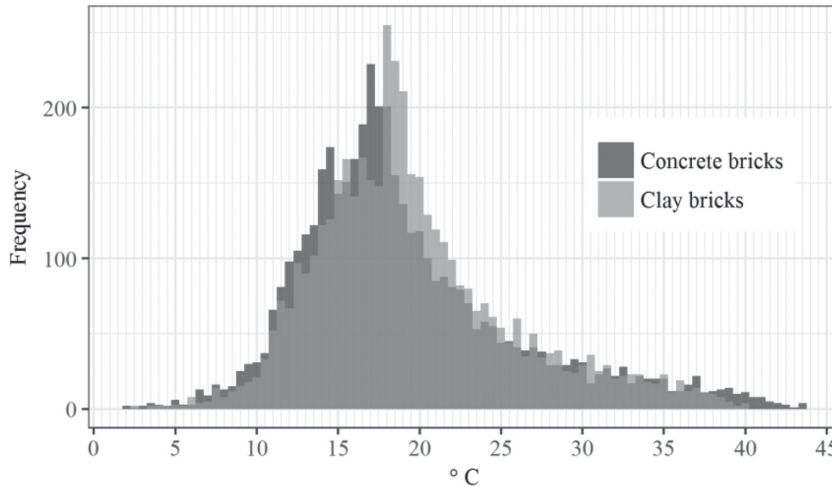

Figure 8: Histogram of the internal surface temperatures over the heating season.

An infrared picture of the internal surface of the wall is shown in Fig. 9. The picture clearly demonstrates the negative effect of the frame and dividers of the glazing unit, casting shadow on the absorber. The lower temperatures of the shaded sections of the external surface result in lower temperature regions on the internal surface (visible on the picture). This effect is amplified by the relatively high distance between the absorber and the glazing unit. As previously mentioned, this distance should preferably be limited to 2–5 cm, while frame dividers should be minimized. It is also important to reduce to the maximum extent possible the placement of furniture or other objects, which may impede the efficient heat exchange between the solar wall and the occupied space [8, 13].

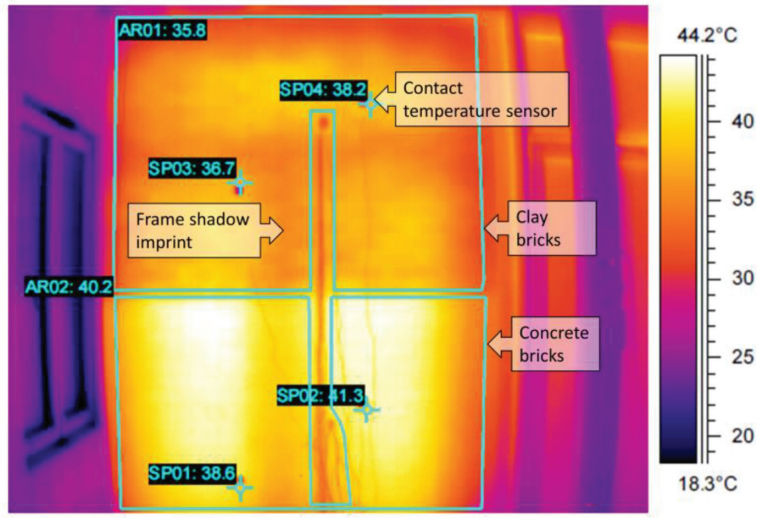

Figure 9: Infrared picture of the internal surface of the solar wall (18/02/2015 16:45).

The measured temperatures and air velocities in the air space, as well as the measured temperatures of the absorber, were used to analyse the heat transfer processes occurring between the absorber and the glazing. The analysis shows that, on the average, heat transfer due to thermal radiation was about four times more intensive than convective heat transfer in the air gap. Calculations show that the use of selective absorber (with an infrared emissivity of 0.11) would reduce the radiant heat transfer approximately seven times, which will result in about 70% reduction of total heat losses [16]. This confirms the high significance of the type of absorber coating on the energy performance of the solar wall, discussed above.

4 CONCLUSIONS

The presented simplified model can be used, along with other analysis tools, to estimate the energy and cost efficiency of an unvented solar wall, especially in the early stages of the building design process. The simplified model is robust and suitable for a wide range of climatic conditions. It provides rather conservative results and should not overestimate the efficiency of a typical solar wall. The results of the study show that in temperate and warm climates, the application of solar walls can improve building energy performance, if they are designed according to the best practices and are well combined with other elements of passive solar design.

ACKNOWLEDGEMENTS

This work has been supported by The National Science Fund of Bulgaria under projects number ДУНК-01/3 (DUNK-01/3) and ДФНИ Е 02/17 (DFNI E 02/17).

REFERENCES

[1] Trombe, F. & Michel, J., *Naturally air-conditioned dwellings*, U.S. Patent 3832992, 1972.

[2] Morse, E.S., *Warming and ventilating apartments by sun's rays*, U.S. Patent 246626, 1881.

[3] Duffie, J. & Beckman, W., *Solar engineering of thermal processes*, 3rd ed, Wiley: Hoboken, New Jersey, pp. 733–759, 2006.

[4] Wilson, A., *Thermal storage wall design manual*, New Mexico Solar Energy Association: Albuquerque, New Mexico, 1979.

[5] Monsen, W.A., Klein S.A. & Beckman, W.A., The un-utilizability design method for collector-storage walls. *Solar Energy*, **29**, pp. 421–429, 1982. https://doi.org/10.1016/0038-092x(82)90079-2

[6] Saadatian, O., Sopian, K., Lim, C.H., Asim, N. & Sulaiman, M.Y., Trombe walls: a review of opportunities and challenges in research and development. *Renewable and Sustainable Energy Reviews,* **16**, pp. 6340–6351, 2012. http://dx.doi.org/10.1016/j.rser.2012.06.032

[7] De Gracia Cuesta, A., *Thermal analysis of a ventilated facade with phase change materials (PCM)*, PhD thesis, University of Lleida, Spain, 2013.

[8] Torcellini, P., Long, N., Pless, S. & Judkoff, R., *Evaluation of the low-energy design and energy performance of the Zion National Park Visitors Center,* NREL/TP-550-34607, NREL: Golden, Colorado, 2005.

[9] Torcellini, P. & Pless, S., Trombe walls in low-energy buildings: Practical experiences, Presented at *8th World Renewable Energy Congress and Expo*, Denver, Colorado, 2004.

[10] Judkoff, R. & Sokol, F., Performance of a selective-surface Trombe wall in a small commercial building, Presented at *AS/ISES Annual Meeting*, Philadelphia, Pennsylvania, 1981.
[11] Steven Winter Associates, *The passive solar design and construction handbook*, Wiley: New York, 1998.
[12] Dowson, M., Harrison, D. & Dehouche, Z., Trombe walls with nanoporous aerogel insulation applied to UK housing refurbishments. *International Journal of Smart and Nano Materials*, **5**(4), pp. 283–303, 2014. http://dx.doi.org/10.1080/19475411.2014.999730
[13] Torcellini, P., Pless, S., Judkoff, R. & Crawley, D., Solar technologies & the building envelope. *ASHRAE Journal*, **49**(4), pp. 14–22, 2007.
[14] Klein, S.A., Beckman, W.A., Mitchell, J.W., Duffie, J.A., Duffie, N.A., Freeman, T.L., *et al.*, *TRNSYS 17: A transient system simulation program*, University of Wisconsin-Madison, 2010.
[15] TESS Component Library Package. Available at: http://www.trnsys.com/tess-libraries
[16] Stankov, B., *Models of the heat transfer processes in passive solar systems*, PhD thesis, Technical University of Sofia, Bulgaria, 2015.
[17] *Subroutine Type36*, Solar Energy Laboratory, University of Wisconsin-Madison, 2013.
[18] ANSI/ASHRAE/IESNA Standard 90.1-2007, *Energy standard for buildings except low-rise residential buildings*, Atlanta, Georgia, 2007.
[19] Kottek, M., Grieser, J., Beck, C., Rudolf, B. & Rubel F., World map of the Köppen-Geiger climate classification updated. *Meteorologische Zeitschrift*, **15**, pp. 259–263, 2006. https://doi.org/10.1127/0941-2948/2006/0130
[20] EN ISO 13790:2008, *Energy performance of buildings -- Calculation of energy use for space heating and cooling*, Geneva, Switzerland, 2008.
[21] *CIBSE Guide A – Environmental design*, 8th ed., The Chartered Institution of Building Services Engineers: London, United Kingdom, 2015.
[22] ANSI/ASHRAE Standard 55-2010, *Thermal environmental conditions for human occupancy*, Atlanta, Georgia, 2010.